Operating a ^{87}Sr Optical Lattice Clock With High Precision and at High Density

Matthew D. Swallows, Michael J. Martin, Michael Bishof, Craig Benko, Yige Lin, Sebastian Blatt, Ana Maria Rey, and Jun Ye

(*Invited Paper*)

Abstract—We describe recent experimental progress with the JILA Sr optical frequency standard, which has a systematic uncertainty at the 10^{-16} fractional frequency level. An upgraded laser system has recently been constructed in our lab which may allow the JILA Sr standard to reach the standard quantum measurement limit and achieve record levels of stability. To take full advantage of these improvements, it will be necessary to operate a lattice clock with a large number of atoms, and systematic frequency shifts resulting from atomic interactions will become increasingly important. We discuss how collisional frequency shifts can arise in an optical lattice clock employing fermionic atoms and describe a novel method by which such systematic effects can be suppressed.

I. INTRODUCTION

OPTICAL atomic frequency standards based on ultracold neutral atoms trapped in magic wavelength optical lattices have made impressive progress in the few years since their initial proposal [1]. However, such clocks have not yet realized their anticipated accuracy and still lag behind the best optical clocks based on single trapped ions [2], [3]. Because of the reduction in quantum projection noise [4] when a large number of particles are simultaneously interrogated, neutral atom clocks have the potential to surpass single ion clocks in terms of stability. Current ultrastable laser technology is not yet sufficiently advanced to fully realize this advantage, and the stability of current lattice clocks is limited by the optical Dick effect [5] at about the same level at which single ions clocks are limited by quantum projection noise. The Dick effect may be mitigated by operating a lattice clock at high duty cycle [6], but improvements to the stability of the interrogation laser also have a direct influence on clock stabil-

ity. In this article, we will discuss a state-of-the-art laser system recently constructed at JILA.

The quantum projection noise-limited stability of a frequency standard operating with two-pulse Ramsey spectroscopy is given by

$$\sigma_y(\tau) = \frac{1}{2\pi C T \nu_0} \sqrt{\frac{1 - p_e}{p_e} \frac{1}{N} \frac{t_c}{\tau}}, \tag{1}$$

where C is the contrast of the Ramsey fringes, T is the Ramsey interrogation time, ν_0 is the optical transition frequency, p_e is the excited state fraction at the operating points, N is the number of atoms interrogated, t_c is the cycle time, and τ is the averaging time. Using some typical operating parameters for the JILA Sr standard ($T = 0.1$ s, $\nu_0 = 429.228$ THz, $C = 0.5$, $p_e = 0.5$, $N = 5000$, $t_c = 1.0$ s), we find $\sigma_y(\tau) \simeq 1.0 \times 10^{-16}/\sqrt{\tau}$. As laser technology continues to improve and lattice clocks begin to reach the quantum projection noise limit, systematic inaccuracies associated with trapping large numbers of atoms will become a pressing concern. Although spin-polarized fermions do not interact via s-wave scattering, sizable collisional frequency shifts can still occur [7]. We will detail the underlying mechanisms responsible for these effects, and will also discuss a novel method of suppressing collisional frequency shifts by trapping atoms under strongly-interacting conditions, which was recently demonstrated in our laboratory [8].

II. STRONTIUM OPTICAL LATTICE CLOCK

In the JILA Sr optical lattice clock experiments, a sample of ^{87}Sr atoms is prepared by cooling and trapping atoms in an optical lattice using a two-stage magneto-optical trap (MOT). Sr atoms are loaded into the first MOT stage, operating on the strong $^1S_0 \rightarrow {}^1P_1$ transition at 461 nm, from a Zeeman-slowed thermal atomic beam. Approximately 10^6 atoms are cooled to millikelvin temperatures in this "blue" MOT, and are then loaded into a second "red" MOT operating on the narrow (linewidth 7.6 kHz) $^1S_0 \rightarrow {}^3P_1$ intercombination transition at 689 nm, where they are cooled to temperatures of just a few microkelvin. During the second MOT stage, atoms are loaded into an optical lattice formed by a vertically-oriented standing wave laser field which is overlapped with the atoms. This lattice is tuned to the magic wavelength

[9] for the $^1S_0 \rightarrow {}^3P_0$ optical clock transition, at which ac Stark shifts of the lower and upper clock states are equal. The $^1S_0 \rightarrow {}^3P_0$ clock transition is highly forbidden in bosonic alkaline-earth isotopes, but is weakly allowed in fermionic species because of hyperfine-induced mixing, with an estimated linewidth of ~1 mHz [10], [11], [12]. Following the MOT-cooling stages, atoms are optically pumped to a single nuclear spin state, and may be further cooled in the lattice via Doppler and sideband cooling procedures [13]. The clock transition is then interrogated with an ultrastable laser aligned along the lattice direction, so that the atoms are probed in the Lamb-Dicke and resolved-sideband regimes [13]. After the clock interrogation, the population in the $^1S_0$ state is destructively detected by observing atomic fluorescence due to a probe beam on the strong 461-nm transition; the population in the $^3P_0$ state is then measured by first optically pumping those atoms to the ground state and then detecting their fluorescence when exposed to the probe beam. The ultrastable laser system used in most of the experiments described in this article was detailed in [14]. Recently, a significantly improved laser system was constructed in our laboratory; it will be discussed in Section III.

The estimated error of the JILA Sr optical frequency standard is given in Table I. Many of the systematic effects listed are expected to be controllable at the sub-10^{-17} level. The magic wavelength is known to within a 5-MHz uncertainty, permitting control of the differential Stark shift due to the optical lattice at the 1.0×10^{-17} level with a trap depth of ~20 μK [15] (the -6.5×10^{-16} correction was applied to the clock frequency because the optical lattice was operated slightly away from the magic wavelength in [16], [17]). Higher-order effects (hyperpolarizability effects and magnetic dipole (M1)/electric quadrupole (E2) polarizability effects [18]) as well as vector and tensor components of the electric dipole (E1) polarizability have also been found to be manageable at the 10^{-17} level or better [15]. The first-order Zeeman effect (as well as vector polarizability effects) can be addressed by averaging the clock transition frequency for two different projections of the nuclear spin [17]. The BBR shift is obviously the largest single frequency shift affecting the Sr clock transition. Improved knowledge of several key atomic transition rates [19] or measurements of the differential static polarizability [20] should enable a more precise calculation of the shift, but any room temperature clock experiments must contend with experimental uncertainties in the ambient BBR environment. Spectroscopy of Rydberg transitions from the $^3P_0$ state has recently been proposed as a method of *in situ* temperature determination [21]. Because the BBR shift scales with the fourth power of the temperature, interrogating the Sr clock transition in a cryogenically-cooled region may provide a solution to this problem [20]. The other primary contribution to the error budget of the JILA standard comes from atomic density-dependent collisional interactions. These collisional frequency shifts can occur despite the fact that the JILA standard is based on ultracold fermions [7]. We

TABLE I. Systematic Frequency Shifts and Their Uncertainties for the ^{87}Sr Frequency Standard (as in [16]).

Contributor	Correction ($\times 10^{-16}$)	Uncertainty ($\times 10^{-16}$)
Lattice Stark (scalar/tensor)	−6.5	0.5
Hyperpolarizability (lattice)	0.1	0.1
Blackbody radiation Stark	54.0	1.0
AC Stark (probe)	0.2	0.1
First-order Zeeman	0.2	0.2
Second-order Zeeman	0.36	0.04
Density	3.8	0.5
Line pulling	0	0.2
Servo error	0	0.5
Second-order Doppler	0	≪0.01
Systematic total	52.1	1.36

will detail how collisional shifts can arise in such a clock in Section IV and describe a method by which they are controllable at the 10^{-17} level.

III. Ultrastable Laser System

At the heart of any optical frequency standard lies an ultrastable laser system. The remarkable short-term performance of the best of these systems, which has been demonstrated to be at the low 10^{-16} instability level [22], [23], allows hertz-level resolution of the ultra-narrow optical transitions used in optical standards. It is this same short-term stability that determines the performance of optical standards up to the 10-s range. Depending on the type of spectroscopy and experimental sequence used, the long-term stability of optical clocks is crucially dependent on the frequency noise spectrum of the local oscillator laser via the optical Dick effect [24]. The current development of next-generation ultrastable laser systems, both at JILA and elsewhere, will allow the full signal-to-noise benefit of using thousands of neutral atoms to be realized.

To this end, we have designed a cavity-stabilized laser system to be used as the new local oscillator of the JILA Sr optical lattice clock, comprised of an external cavity diode laser locked to the stable reference cavity shown in Fig. 1. The optical characteristics of the cavity are determined by the ultra-high reflectivity mirrors, which are the same design as those used in [14] with fused silica substrates. These mirrors are optically contacted to the ultra-low expansion glass (ULE) spacer. We measure a finesse of 190 000, which results in a resonance width of 2 kHz. We have attached additional ULE rings to the back of these mirrors as in [25], whose effect we have modeled to raise the zero-crossing of the ensemble coefficient of thermal expansion (CTE) by ~3°C. We expect the ensemble CTE to be nulled at approximately 17°C, and the cavity is maintained at this temperature. The cavity is enclosed in a two-stage vacuum envelope, and the pressure within the inner vacuum chamber is ~1.3×10^{-6} Pa (~1×10^{-8} torr). A copper heat shield between the cavity and the inner vacuum chamber wall serves to fur-
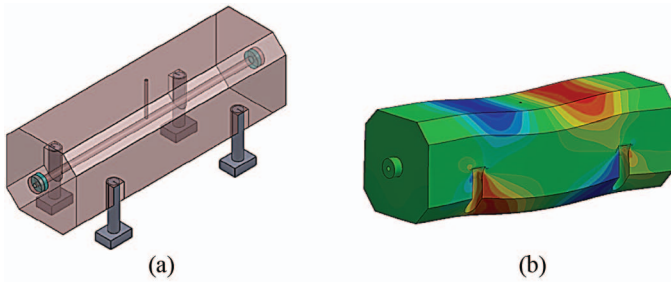
Fig. 1. (a) Mechanical design of the 39.4-cm JILA optical cavity. The support structure comprises Teflon posts of approximately 10 cm in length. The fused silica mirrors (light blue in color) are optically attached to the spacer. Additional ultra-low expansion glass annular rings are attached directly to the back surface of the mirrors. (b) Finite element analysis of the spacer with optimized support conditions and a downward acceleration equal to $1g$, where g is the acceleration of gravity. The relative deformations have been amplified by a factor of $\sim 3 \times 10^9$, with color specifically indicating displacements along the optical axis.
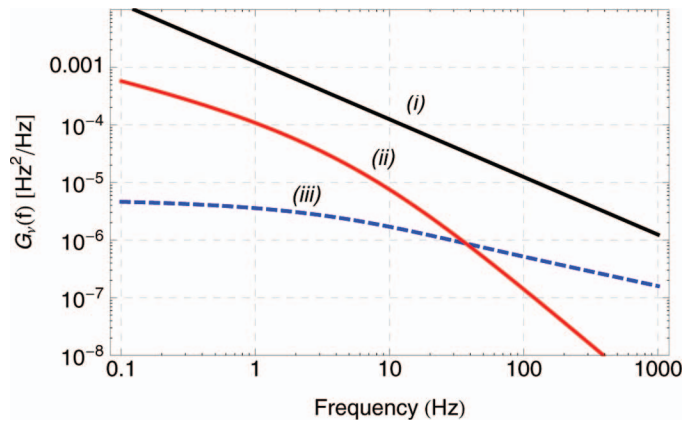

Fig. 2. Thermal noise contributions to the frequency noise power spectral density of a laser stabilized to the cavity presented in Fig. 1: (i) total Brownian motion contribution arising from the cavity spacer, mirror substrates, and mirror coatings, (ii) thermo-elastic noise arising from statistical temperature fluctuations in the mirror substrate, and (iii) thermo-optic noise arising from temperature fluctuations in the mirror coating driving optical length changes through both thermal expansion and the thermo-refractive index change of the mirror coating.

ther reduce the feedthrough of external temperature fluctuations. With millikelvin-level stability on our vacuum chamber and a two-day thermal time constant between the chamber and the cavity, the temperature-induced fluctuations of the laser drift are at the 5 mHz/s level over an hour time scale. Relative to our previous ultrastable laser system [14], this represents an approximately 100-fold improvement in the predictability of the drift over experimental timescales.

To overcome the well-known problem of mirror and substrate Brownian thermal noise [26], [27], we have chosen to use a much longer cavity for laser stabilization in comparison to our previous systems. The new system is 39.4 cm in length, compared with the 7 cm length of the previous-generation system [14]. Additionally, we have chosen to use fused silica mirror substrates as opposed to ULE mirror substrates, which give an additional factor of two improvement in the thermal noise due to the mirror substrates. In total, we expect a factor of 10 improvement over the previous system, with a resulting thermal noise floor of 1×10^{-16}. The detailed expected thermal noise spectrum due to Brownian, thermo-elastic, and thermo-optic noise is shown in Fig. 2, and is based on the treatments found in [28]–[31].

To minimize the coupling of vibrations to an optical length change of the cavity, we performed finite element analysis to optimize the cavity mounting configuration [32]. An example of the simulated deformation is shown in Fig. 1(b). The geometry of the ULE cavity spacer was fixed because it had been manufactured at an earlier date for a different application not requiring vibrational insensitivity. Motivated by symmetry considerations, we optimized the support points to minimize sensitivity to accelerations in the vertical direction arising from both mirror displacements and mirror tilts. Our procedure was to vary the support points' longitudinal position and vertical distance from the midplane and numerically calculate the mirror tilt and displacement. By accumulating an array of values corresponding to different support positions, we

were able to use a linear model that described the tilt and displacement about the respective zero-crossings to extrapolate the optimal positions. Such an extrapolation is desirable in that it can reduce sensitivity errors arising from numerical imprecision.

At the optimized support condition, numerical predictions of vibrational coupling to fractional length change in the horizontal direction was found to be small, at the level of $8 \times 10^{-11}/g$, where g is the acceleration of gravity. However, the mirror tilt sensitivity in this direction is uncompensated, meaning horizontal accelerations cause mirror angular displacement at the level of 40 nrad/g, which further increases vibrational sensitivity if the optical mode does not lie in the geometric center of the cavity [33]. Finally, sensitivity to vibrations in the longitudinal direction can also occur, primarily due to asymmetries in the mounting structure and mirror positions, which couples mirror tilt to optical path length changes.

By applying an oscillating force to the platform on which the laser cavity sits, we have measured the vibrational sensitivity by monitoring the frequency noise spectrum of the beat between this system and a second ultrastable laser system with stability at 1×10^{-15} [14]. We find that the extrapolated DC vibrational sensitivity is at the $1.4 \times 10^{-9}/g$ level for accelerations applied nominally in the vertical direction. We estimate that a 1 mm error in the placement of the cavity support structures leads to an increase of the acceleration sensitivity of $\sim 1 \times 10^{-10}/g$, and therefore such errors are not likely to be the cause of the discrepancy between our modeling and the measured performance. It is possible that the applied oscillatory force had a small component in the horizontal plane, to which our accelerometer was not sensitive.

Although the sensitivity of $1.4 \times 10^{-9}/g$ is an order of magnitude from the state of the art [34], [35], it is nevertheless adequate to reach the thermal noise limited fre-
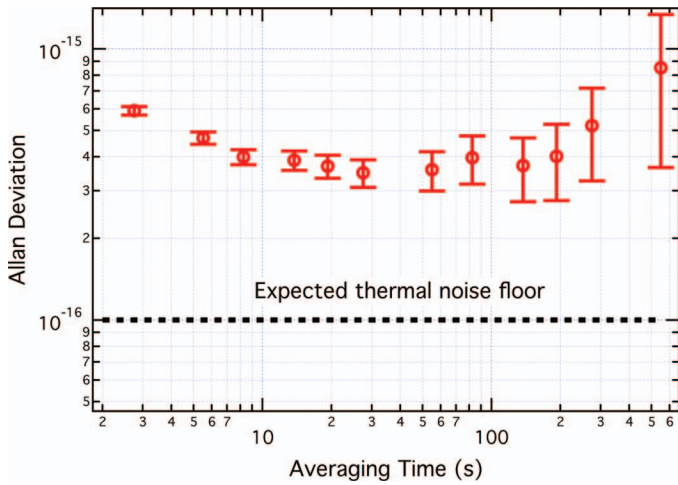
Fig. 3. Allan deviation of fractional frequency corrections applied to the clock laser to keep it on resonance with the ultra-narrow ^{87}Sr $^1S_0 \to {}^3P_0$ clock transition.

Fig. 4. Ultra-narrow atomic resonance scan obtained by superimposing 25 individual scans, each comprising 40 points. The Rabi π-pulse duration was 1 s. By combining scans in this way, slow frequency excursions are removed, and the lineshape information is retained and better resolved via averaging. The figure inset shows representative single-scan data, with no averaging.

quency noise spectrum in the 0 to 5 Hz range with our expected vibration spectrum of ~50 ng/$\sqrt{\text{Hz}}$, given by the noise level of the commercial active vibration cancellation platform on which the cavity is mounted. Additionally, the cavity length of 39.4 cm is, to our knowledge, the physically longest cavity in operation, a factor of five times larger than our previous cavity with vibrational sensitivity of $6 \times 10^{-10}/g$. Given that fractional sensitivity scales with length and the additional complication that our system is mounted horizontally, we find our measured sensitivity to be a favorable validation of our design approach.

To test the performance of the new cavity-stabilized laser system, we used the ultra-narrow $^1S_0 \to {}^3P_0$ clock transition in the ^{87}Sr optical lattice clock. We locked the laser to the $m_F = +9/2$ resonance in the presence of a small bias magnetic field and recorded the shot-by-shot correction signal applied by a digital servo system to the laser frequency (see Fig. 3). At the beginning of the measurement, we applied a constant drift to cancel the intrinsic material relaxation effect of ULE. The correction signal therefore was an estimator of all laser noise with the linear drift removed, and with the additional detection noise of the atomic system comprising photon and atomic shot noise (quantum projection noise) in addition to other technical sources of detection noise. We were able to observe ~10 minute periods of time where the laser frequency excursions were bounded below 1 Hz. The Allan deviation of the correction signal reaches 3.5×10^{-16} at the 30-s time scale before rising again because of the few millihertz per second of uncancelled drift. It is important to note that at short time scales, the noise averages down as white frequency noise, which can arise from the aforementioned detection noise issues in addition to the optical Dick effect [24]. The deviation of the correction signal rises again at longer times, which we attribute to longer-term drift in the cavity resonance frequency. We emphasize that
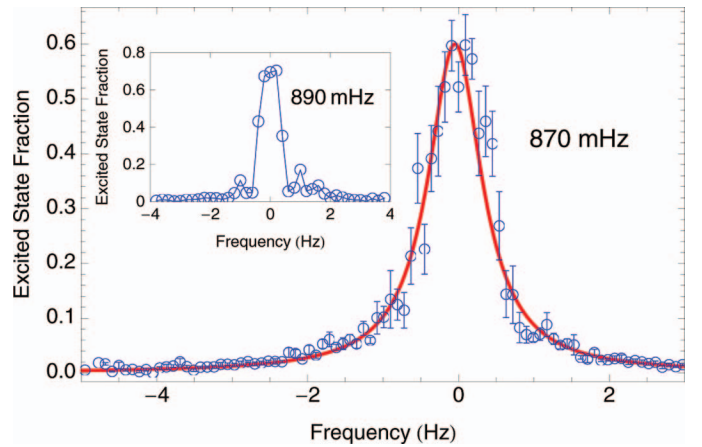
these measurements represent an upper limit to the stability of our new laser system.

A final test of the laser performance was achieved by optically pumping all atoms to a single nuclear spin state in the presence of a small bias field, and directly scanning the stabilized laser across the clock transition with an interrogation time of 1 s. The laser power was chosen to achieve maximum excitation on resonance, consistent with a Rabi π pulse. (The maximum excitation fraction is limited by elastic and inelastic interactions, as well as by inhomogeneous excitation; see Section IV.) We performed spectroscopy on an intentionally dilute atomic sample at our coldest achievable temperature of 1 μK to reduce any potentially detrimental density-dependent broadening. In Fig. 4, we combine 25 consecutive line scans by centering each scan at zero detuning and furthermore bin the combined data using a 90 mHz bin size. The re-centering between scans serves to remove large frequency excursions due primarily to the $1/f$ character of the laser frequency noise. The result, shown in Fig. 4, has a linewidth of 870 mHz, which is close to the expected 800 mHz Fourier limit for Rabi spectroscopy with a 1-s interrogation pulse.

IV. COLLISIONAL SHIFTS IN A FERMION LATTICE CLOCK

Collisions between atoms occupying the same lattice site may lead to both a broadening and a shift of the clock resonance [36]. These effects can be mitigated by operating the lattice clock with ultracold fermionic atoms; at temperatures of a few microkelvin, $l \geq 1$ partial wave scattering is suppressed by the centrifugal barrier in the interatomic potential, and $l = 0$ partial wave scattering is forbidden for identical fermions. This Pauli-blocking of fermionic collisions occurs because the total wave function must be antisymmetric under the exchange of any two particles; if the particles are initially prepared in the
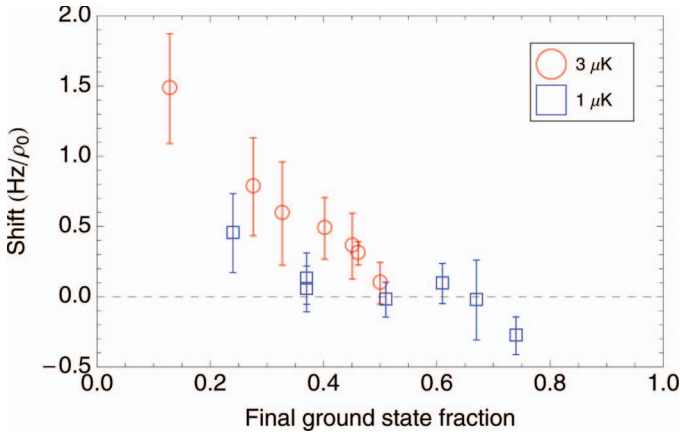
Fig. 5. Density shift measurements in a 1-D optical lattice clock. The inverted clock transition $^3P_0 \rightarrow {}^1S_0$ was interrogated by Rabi spectroscopy, using a sample of spin-polarized atoms. The sample temperature was varied between 1μK and 3μK. The shift is plotted as a function of final ground state fraction after the interrogation pulse. The final ground state fraction is a function of the detuning of the laser from the center of the clock resonance. The data are scaled to a common reference density, $\rho_0 = 1 \times 10^{11}$ cm^{-3}.

same internal state, then their spatial wave function must be antisymmetric, and thus s-wave scattering processes do not occur.

Despite these arguments, a large collisional shift was observed at JILA in a system of ultracold fermions polarized to a single nuclear spin state [7]. In that work, atoms were trapped in a 1-D optical lattice at the magic wavelength, and the clock transition was interrogated using Rabi spectroscopy. The optical clock frequency was measured against the cold Ca optical frequency standard at NIST, as in [17]. The collisional shift was measured by varying the number of atoms loaded into the lattice and observing a shift in the clock resonance. The shift was characterized as a function of the detuning of the locking points from the center of the resonance, which determines the average excited state fraction at the end of the pulse (see Fig. 5). Shifts of the clock transition frequency at the 10^{-15} fractional level were observed. These results were explained using a simple mean field model of the dynamics, as detailed in [37]. If, during interrogation of the clock transition, the optical coupling strength is different for different atoms, then the atoms will evolve into a different superposition of the two clock states, and conditions for complete Pauli blocking are not satisfied. Instead, the atoms experience a mean field shift of the transition frequency that depends on their degree of mutual distinguishability, as quantified by the two-body correlation function. The mean field shift then manifests as a time-dependent shift of the resonance frequency during the course of the Rabi interrogation. This model does predict a zero-crossing of the shift near a final excited state fraction of 50%, which was consistent with the experimental measurements. However, the simple mean field model is not in quantitative agreement with the data, and several more sophisticated theoretical treatments of col-

lisional shifts in a fermion system have been presented in the literature [38]–[41].

The inhomogeneous coupling described previously can occur fairly easily in an optical lattice clock. In a trap, the atom-clock laser coupling is a function of the vibrational modes occupied by the atoms [42]. In a one-dimensional (1-D) optical lattice clock, atoms are typically sufficiently cold that only the lowest one or two vibrational modes along the lattice direction are appreciably populated. However, the trap is relatively weak along the transverse directions, and atoms occupy many transverse vibrational modes. In this case, if the clock laser wave vector has a component along the transverse directions (if it is not perfectly aligned with the 1-D lattice), then the Rabi frequency of the atoms, and thus the degree of coupling inhomogeneity, becomes a function of the degree of misalignment and the ratio of the sample temperature to the transverse vibrational energy spacing [37]. If some misalignment between the clock laser and the lattice exists, or the atoms are not sufficiently cold that only the ground state of the lattice is occupied, then the optical excitation will be inhomogeneous, potentially leading to sizable collisional frequency shifts.

In the rest of this article, we follow the treatment of references [38] and [39]. We consider two particles on the same lattice site, undergoing laser interrogation and colliding with one another. Assuming that the vibrational quantum numbers of the particles are conserved during the collision/interrogation process, the Hamiltonian for the two-particle system can be written in a four-state pseudospin basis set, comprised of three symmetric states with total pseudospin $S = 1$ (the triplet states), and an antisymmetric state with $S = 0$ (the singlet),

$$
\begin{aligned}
|S = 1, M = -1\rangle &\equiv |gg\rangle \\
|S = 1, M = +1\rangle &\equiv |ee\rangle \\
|S = 1, M = 0\rangle &\equiv \frac{1}{\sqrt{2}}|ge + eg\rangle \\
|S = 0, M = 0\rangle &\equiv \frac{1}{\sqrt{2}}|ge - eg\rangle.
\end{aligned}
\tag{2}
$$

In this basis and under the rotating wave approximation, the Hamiltonian H of the system can be written as

$$
H = \begin{pmatrix}
+\delta & 0 & \bar{\Omega}/\sqrt{2} & \Delta\Omega/\sqrt{2} \\
0 & -\delta & \bar{\Omega}/\sqrt{2} & -\Delta\Omega/\sqrt{2} \\
\bar{\Omega}/\sqrt{2} & \bar{\Omega}/\sqrt{2} & 0 & 0 \\
\Delta\Omega/\sqrt{2} & -\Delta\Omega/\sqrt{2} & 0 & U_{eg}
\end{pmatrix}.
\tag{3}
$$

The inhomogeneous coupling is parameterized by the Rabi frequencies $\Omega_{1,2}$ of the two particles; $\bar{\Omega} = (\Omega_1 + \Omega_2)/2$ is the average of the two particles' Rabi frequencies and $\Delta\Omega = (\Omega_1 - \Omega_2)/2$ is half of their difference. The detuning of the coupling laser from exact (zero-density) resonance is δ, and U_{eg} is an interaction energy due to s-wave collisions. If the two particles' coupling strength is the same, then a system initially prepared in the triplet manifold (e.g., in
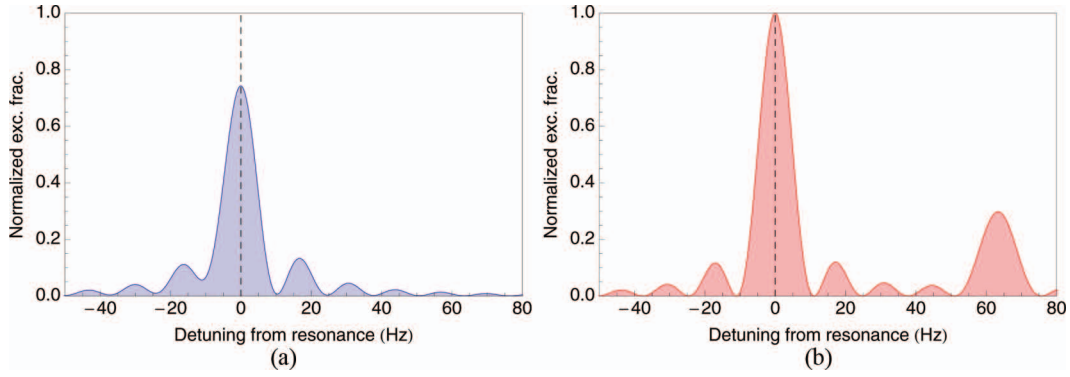
Fig. 6. Lineshapes obtained by numerical solution of Schrödinger equation with the Hamiltonian (3), for $\bar{\Omega} = 40$ s^{-1} and $\Delta\Omega/\bar{\Omega} = 0.16$. (a) Weakly-interacting particles ($U_{eg} = 0.6\bar{\Omega}$): the singlet amplitude is excited by a clock laser tuned near the triplet resonance, leading to an asymmetric lineshape and a density-dependent frequency shift. (b) Strongly-interacting particles ($U_{eg} = 10\bar{\Omega}$): the singlet amplitude is excited only when the clock laser is detuned from the main resonance, appearing as a sideband. In this case, the singlet resonance has minimal influence on the lineshape at small detunings, and thus the density-dependent frequency shift is suppressed. Both lineshapes are unit normalized; the higher peak excitation in (b) is due to the shift of the singlet resonance away from the carrier. The frequency shift of the lineshape in (a) is about -200 mHz, or -4.5×10^{16} in fractional frequency units, whereas the shift of the lineshape in (b) is only about -7 mHz, or -1.6×10^{17} in fractional units, for a locking modulation width of 10 Hz (the frequency shift depends on the width of the frequency modulation used to interrogate both sides of the resonance). The sign of the shift is actually negative for both sets of parameters considered here, due to interference effects between the singlet and triplet excitation pathways. If a thermal average was taken, these effects would average away and one would recover the sign of the shift expected from the simple line-pulling argument (see [39] for more details). Although U_{eg} is positive here, the sideband features observed experimentally occur at negative detunings from resonance.

the $|gg\rangle$ state) will remain in that manifold. Conversely, if the coupling is inhomogeneous, then a finite singlet amplitude will be excited, leading to a density-dependent asymmetry of the resonance.

Lineshapes obtained by numerical integration of the Schrödinger equation using the Hamiltonian (3) are presented in Fig. 6. In the presence of inhomogeneity, the energy scale represented by U_{eg} becomes relevant. If $U_{eg} \leq \bar{\Omega}$, as in Fig. 6(a), then the singlet amplitude can be efficiently excited, potentially leading to large collisional frequency shifts of the clock transition. However, if interactions are strong ($U_{eg} \gg \bar{\Omega}$), then excitation of the singlet is suppressed, and only becomes appreciable when the clock laser detuning matches the energy splitting of the dressed state ($U_{eg} \simeq \sqrt{\bar{\Omega}^2 + \delta^2}$). In this case, a singlet resonance appears that is separated from the carrier, a so-called interaction sideband [43]. This situation is depicted in Fig. 6(b).

Experimentally-observed lineshapes [43] in both 1-D and 2-D lattices (see subsequent discussion) are shown in Fig. 7. These lineshapes were obtained by scanning the ultrastable laser frequency across the clock resonance several times and averaging the atomic response at each detuning. To account for the effect of laser drift, each scan was centered by fitting a Lorentzian function to the atomic response before averaging (we note that these data were taken using our older ultrastable laser system; with our upgraded system, similar spectra are obtained in a single scan). In a 1-D lattice, the lineshape is well approximated by the Rabi solution to the problem of a driven two-level system. However, in the 2-D lattice, strong interactions in multiply-occupied sites lead to the sideband-like features at negative detuning. In current experiments, these sidebands are broadened because of the variation of site oc-

cupation number and the thermal distribution of occupied vibrational modes within a site, but in degenerate gases of alkaline earth atoms they are predicted to be narrow and may be useful as precision probes of interaction parameters and occupation number (see reference [43] and associated supporting online material).

The sideband picture also points toward a novel method of suppressing the collisional shift in an optical lattice clock. If the interactions are strong, or can be engineered to be so, then the interaction sidebands will be well-re-
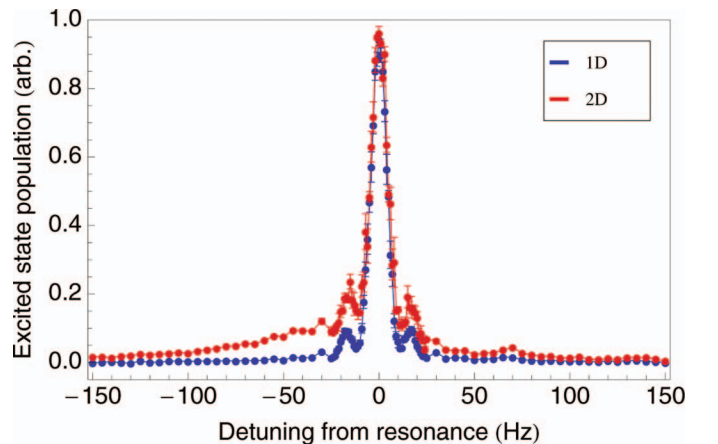

Fig. 7. Interaction sidebands in the strongly-interacting and weakly-interacting regimes. For each lineshape, several traces are averaged together to reduce the effects of laser noise, and the resulting lineshapes are normalized to their peak value. In a 1-D lattice, the lineshape is well-approximated by the classical Rabi solution to the problem of a two-level atom. In a 2-D lattice, sidebands appear due to interactions in multiply-occupied lattice sites. If interactions are strong enough, then these sideband features will be entirely resolved from the carrier and the collisional shift can be suppressed.

solved and any line pulling associated with them will have minimal impact on the carrier resonance. By trapping ^{87}Sr atoms in a 2-D optical lattice, we were able to reach this strongly-interacting regime and observe a marked suppression of the collisional shift [8]. In that work, atoms were first loaded into a 1-D optical lattice, and a second nearly-orthogonal lattice was adiabatically established in the same spatial region. After loading of the 2-D lattice, the original 1-D lattice was ramped off and then on again, to remove any atoms trapped in the region outside the overlap of the two beams. The two lattice beams were co-polarized to eliminate the possibility of vector or tensor shifts of the clock transition [15]. The two beams were detuned from one another by 200 MHz to eliminate interference effects, and were detuned by ±100 MHz from the magic wavelength. This large detuning was chosen for reasons of experimental convenience, and in a true 2-D optical lattice clock the detuning could be made much smaller, or the two beams could be phase-stabilized and operated exactly at the magic wavelength. The loading conditions were such that the majority of lattice sites were singly occupied, but in sites occupied by more than one atom (~20% to 30% of lattice sites) the local density was an order of magnitude larger than in a 1-D lattice at comparable temperature. The density shift was measured by servo-controlling the clock laser to the atomic clock resonance while the number of atoms loaded into the lattice was varied on a short time scale. The averaged difference in the frequency of the locked clock laser under the two density conditions is a measurement of the shift. When undertaking such a differential measurement, it is important that nothing but the particle density varies between the two experimental conditions, or a systematic effect could mimic the density-dependent shift. In these experiments, the density was modulated by varying the rate at which atoms were loaded into the first stage MOT (the loading rate was varied by changing the power in a laser beam that slowed atoms from the thermal atomic beam source; this beam was mechanically shuttered during interrogation of the clock transition). We emphasize that the particle density was not varied by changing the timing of the experimental sequence, as would be the case if the loading time of the MOT was varied. At lower trap depths and at higher temperatures, large density-dependent frequency shifts were observed (even at the lowest trap depths investigated, the particle density in multiply-occupied lattice sites was still significantly larger than in a 1-D lattice). At the lowest temperatures investigated and with sample sizes of 1000 to 2000 atoms, no collisional shift was observed, with an uncertainty of 1.7×10^{-17} (Fig. 8). The sample temperature was not observed to depend on the sample density. A complete theoretical model of s-wave collisional frequency shifts in a strongly-interacting lattice clock is presented in [8] and in the accompanying supporting online material. It is worth noting that, in this strongly-interacting regime, the splitting of the singlet resonance from the carrier increases as more atoms are loaded into a

lattice site, and therefore the atomic density shift can be increasingly suppressed as the particle number increases.

Recently, evidence of residual p-wave interactions was observed in a Yb optical lattice clock at a temperature of 10μK [44]. If p-wave interactions are important, then the two-particle Hamiltonian (3) possesses additional diagonal interaction terms V_{gg}, V_{ee}, and V_{eg} in the triplet manifold, which lead to a bosonic excitation spectrum:

$$H = \begin{pmatrix} V_{gg} + \delta & 0 & \bar{\Omega}/\sqrt{2} & \Delta\Omega/\sqrt{2} \\ 0 & V_{ee} - \delta & \bar{\Omega}/\sqrt{2} & -\Delta\Omega/\sqrt{2} \\ \bar{\Omega}/\sqrt{2} & \bar{\Omega}/\sqrt{2} & V_{eg} & 0 \\ \Delta\Omega/\sqrt{2} & -\Delta\Omega/\sqrt{2} & 0 & U_{eg} \end{pmatrix}. \quad (4)$$

In this case, atoms initially prepared in $|gg\rangle$ are coupled to the $S = 1$, $M = 0$ state when the laser detuning matches $V_{eg} - V_{gg}$, and a two-photon resonance occurs when $\delta = 1/2(V_{ee} - V_{gg})$. The excitation spectrum may still display s-wave interaction sidebands, but the carrier resonance itself will be shifted and broadened in a density-dependent manner. Although the Sr–Sr p-wave centrifugal barrier is estimated to be >25μK and the JILA Sr lattice clock is typically operated at temperatures of just a few microkelvin, we have evidence that these interactions play an important role in ultracold Sr collisions. Further investigation of the role of p-wave interactions in a Sr system is currently under way.

V. Conclusion

State-of-the-art ultrastable laser systems may allow operation of an optical lattice clock at the stability limits set by quantum projection noise. Such a clock, operating with several thousand atoms, could exhibit a stability of $\sim 1 \times 10^{-16}/\sqrt{\tau}$. Avoiding collisional frequency shifts at large particle densities will be challenging, but operating a lattice clock in the strongly-interacting regime may, paradoxically, reduce or eliminate systematic frequency shifts due to atomic interactions.

Appendix

In the JILA experiments, the optical lattice is loaded from a MOT operating on the $^1S_0 \rightarrow {}^3P_1$ transition. The lattice is overlapped with the MOT atomic cloud, which has an approximately Gaussian spatial distribution with a standard deviation $\sigma_{\text{cloud}} \simeq 30$ μm. We therefore assume that atoms are distributed across lattice sites according to a Poissonian distribution with a mean particle number per site given by the Gaussian spatial distribution of the MOT.

The mean number of particles at lattice site i is

$$G(i) = \frac{N_0}{\sqrt{2\pi\sigma_l^2}} \exp\left[-\frac{i^2}{2\sigma_l^2}\right], \quad (5)$$

where N_0 is the total number of atoms loaded, i is the site index (which can take both positive and negative values
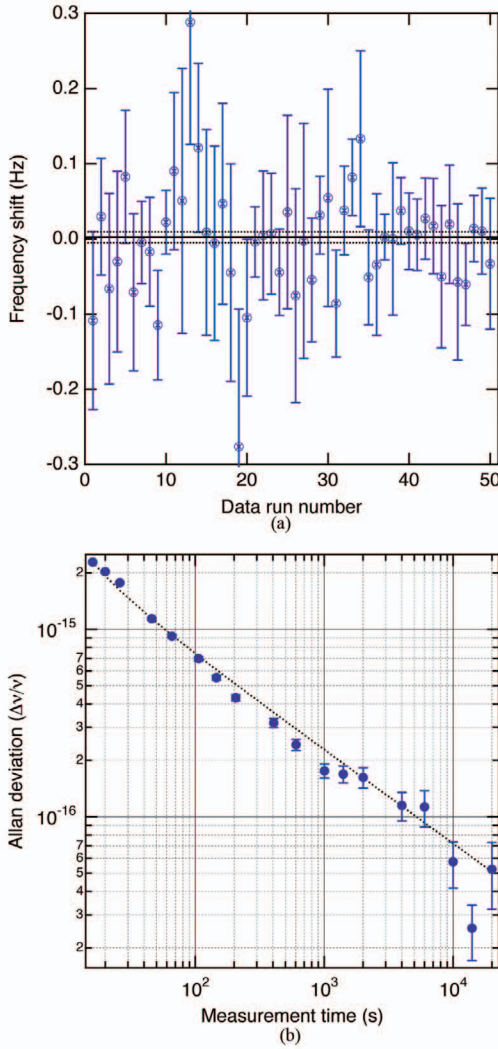
Fig. 8. Density shift measurements in a strongly-interacting lattice clock. (a) Measurement record. Each point represents a period of continuous lock while the particle density was being modulated, with error bars determined from the standard error of shift measurements during the lock period. The weighted mean (solid line) and error (dashed lines) of all points was $(0.6 \pm 1.7) \times 10^{-17}$ at a particle number of ~1000 atoms, and $\sqrt{\chi_{\text{red}}^2} = 0.73$. (b) Allan deviation of the shift measurements from (a), ignoring dead time between measurements, displaying white noise behavior.

and is equal to zero at the center of the atom cloud), and $\sigma_l = \sigma_{\text{cloud}}/(\lambda_l/2)$ is the standard deviation of the MOT cloud in units of lattice half-wavelengths. The probability of n particles occupying lattice site i is then given by the Poisson distribution

$$P(i,n) = e^{-G(i)} \frac{G(i)^n}{n!}. \qquad (6)$$

The expected site occupancy for the JILA experiment (and in the inset, the fraction of the population with a given site occupancy) are plotted in Fig. 9.
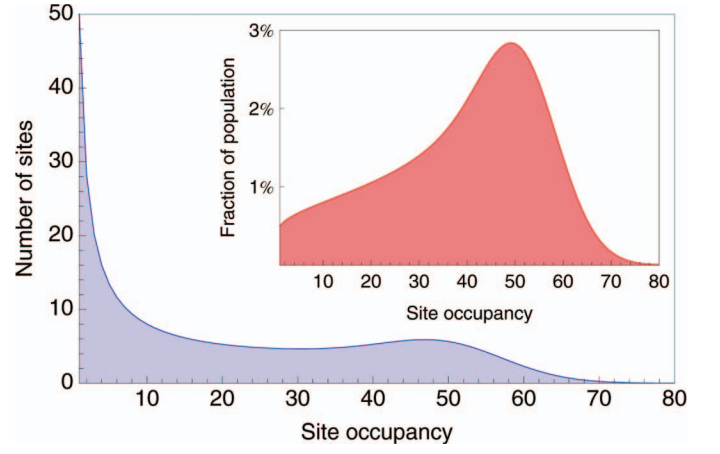

Fig. 9. Expected site occupancy for the JILA experiments with $N_0 \sim 10^4$ atoms. When the lattice is loaded from a magneto-optical trap with a characteristic dimension $\sigma_{\text{cloud}} = 30$ μm, approximately 440 lattice sites are occupied and the average number of atoms per site is ~22.6. The largest fraction of the total population is contained in sites with occupation number ~50.

Assuming a Boltzmann thermal distribution, the spatial distribution of particles in the harmonic potential of a lattice site is also Gaussian:

$$n(\mathbf{r}) = \frac{N_{\text{site}}}{\pi^{3/2}L_x L_y L_z} \exp\left(-\frac{x^2}{L_x^2} - \frac{y^2}{L_y^2} - \frac{z^2}{L_z^2}\right), \qquad (7)$$

where N_{site} is the number of particles occupying the site, and $L_{j=x,y,z}$ are the $1/e$ widths given by

$$L_j = \sqrt{\frac{\hbar}{2\pi m \nu_j}} \times \sqrt{2\langle n_j \rangle + 1}, \qquad (8)$$

where m is the Sr mass, ν_j is the trap oscillation frequency along $\hat{j}$, and

$$\langle n_j \rangle = \left(\exp\left[\frac{h\nu_j}{k_B T}\right] - 1\right)^{-1} \qquad (9)$$

is the average vibrational quantum number in the $\hat{j}$ direction. This expression has the virtue that it smoothly interpolates between the high temperature $(k_B T > h\nu_j)$ limit where the atomic distribution is Gaussian, and the low temperature $(k_B T \leq h\nu_j)$ limit where mostly the ground state of the trapping potential is occupied and the atomic distribution is given by the zero-point wave function with a characteristic width $\hbar/(2\pi m \nu_j)$. The density averaged over a lattice site is given by the density-weighted density,

$$\begin{aligned} \bar{n} &= \frac{1}{N_{\text{site}}} \int n(\mathbf{r})^2 \mathrm{d}\mathbf{r} \\ &= \frac{N_{\text{site}}}{(2\pi)^{3/2} L_x L_y L_z}. \end{aligned} \qquad (10)$$

In the JILA 1-D optical lattice clock, with trapping frequencies $\nu_z = 80$ kHz and $\nu_{x,y} = 450$ Hz, and typical tem-

peratures of $T_{x,y,z} \simeq 3\mu K$, the density per particle is ρ_{particle} = 1.7×10^{10} cm^{-3}. With 10^4 particles loaded into the optical lattice, the average site occupancy is $\bar{N}_{\mathrm{site}} \simeq 23$, so that the average site has a particle density of $\bar{\rho}_{\mathrm{site}} = 3.9 \times 10^{11}$ cm^{-3}.

For purposes of comparison, the Sr optical lattice clock at LNE-SYRTE loads atoms directly from a larger MOT cloud, $\sigma_{\mathrm{cloud}} = 700$ μm, operating on the $^1S_0 \rightarrow {}^1P_1$ transition, and these atoms are loaded into a lattice with trapping frequencies $\nu_z = 120$ kHz and $\nu_{x,y} = 250$ Hz, at temperatures $T_z \simeq 4\mu K$, $T_{x,y} \simeq 15\mu K$ [45]. Following the same procedures as previously given, we estimate that the density per particle is $\rho_{\mathrm{particle}} = 1.4 \times 10^9$ cm^{-3}. With 10^4 particles loaded into the optical lattice, approximately 5200 sites are occupied, and the average site occupancy is $\bar{N}_{\mathrm{site}} \simeq 1.9$. Therefore the average site density is $\bar{\rho}_{\mathrm{site}} = 2.7 \times 10^9$ cm^{-3}, a factor of 145 smaller than in the JILA experiment. The absence of a density shift in the SYRTE experiments [45] is thus consistent with their measurement precision.

References

[1] H. Katori, M. Takamoto, V. G. Pal'chikov, and V. D. Ovsiannikov, "Ultrastable optical clock with neutral atoms in an engineered light shift trap," *Phys. Rev. Lett.*, vol. 91, no. 17, art. no. 173005, Oct. 2003.

[2] C. W. Chou, D. B. Hume, J. C. J. Koelemeij, D. J. Wineland, and T. Rosenband, "Frequency comparison of two high-accuracy Al$^+$ optical clocks," *Phys. Rev. Lett.*, vol. 104, no. 7, art. no. 070802, Feb. 2010.

[3] W. H. Oskay, S. A. Diddams, E. A. Donley, T. M. Fortier, T. P. Heavner, L. Hollberg, W. M. Itano, S. R. Jefferts, M. J. Delaney, K. Kim, F. Levi, T. E. Parker, and J. C. Bergquist, "Single-atom optical clock with high accuracy," *Phys. Rev. Lett.*, vol. 97, no. 2, art. no. 020801, 2006. [Online]. Available: http://link.aps.org/abstract/PRL/v97/e020801

[4] W. M. Itano, J. C. Bergquist, J. J. Bollinger, J. M. Gilligan, D. J. Heinzen, F. L. Moore, M. G. Raizen, and D. J. Wineland, "Quantum projection noise: Population fluctuations in two-level systems," *Phys. Rev. A*, vol. 47, no. 5, pp. 3554–3570, May 1993.

[5] P. Westergaard, J. Lodewyck, and P. Lemonde, "Minimizing the Dick effect in an optical lattice clock," *IEEE Trans. Ultrason. Ferroelectr. Freq. Control*, vol. 57, no. 3, pp. 623–628, 2010.

[6] J. Lodewyck, P. G. Westergaard, and P. Lemonde, "Non-destructive measurement of the transition probability in a Sr optical lattice clock," *Phys. Rev. A*, vol. 79, art. no. 061401(R), 2009.

[7] G. K. Campbell, M. M. Boyd, J. W. Thomsen, M. J. Martin, S. Blatt, M. D. Swallows, T. L. Nicholson, T. Fortier, C. W. Oates, S. A. Diddams, N. D. Lemke, P. Naidon, P. Julienne, J. Ye, and A. D. Ludlow, "Probing interactions between ultracold fermions," *Science*, vol. 324, no. 5925, pp. 360–363, 2009.

[8] M. D. Swallows, M. Bishof, Y. Lin, S. Blatt, M. J. Martin, A. M. Rey, and J. Ye, "Suppression of collisional shifts in a strongly interacting lattice clock," *Science*, vol. 331, no. 6020, pp. 1043–1046, 2011. [Online]. Available: http://www.sciencemag.org/content/331/6020/1043.abstract

[9] J. Ye, H. J. Kimble, and H. Katori, "Quantum state engineering and precision metrology using state-insensitive light traps," *Science*, vol. 320, no. 5884, pp. 1734–1738, 2008. [Online]. Available: http://www.sciencemag.org/content/320/5884/1734.abstract

[10] R. Santra, K. V. Christ, and C. H. Greene, "Properties of metastable alkaline-earth-metal atoms calculated using an accurate effective core potential," *Phys. Rev. A*, vol. 69, no. 4, art. no. 042510, Apr. 2004.

[11] S. G. Porsev and A. Derevianko, "Hyperfine quenching of the metastable $^3P_{0,2}$ states in divalent atoms," *Phys. Rev. A*, vol. 69, no. 4, art. no. 042506, Apr. 2004.

[12] M. M. Boyd, T. Zelevinsky, A. D. Ludlow, S. Blatt, T. Zanon-Willette, S. M. Foreman, and J. Ye, "Nuclear spin effects in optical lattice clocks," *Phys. Rev. A*, vol. 76, no. 2, art. no. 022510, 2007. [Online]. Available: http://link.aps.org/abstract/PRA/v76/e022510

[13] D. Leibfried, R. Blatt, C. Monroe, and D. Wineland, "Quantum dynamics of single trapped ions," *Rev. Mod. Phys.*, vol. 75, no. 1, pp. 281–324, Mar. 2003.

[14] A. D. Ludlow, X. Huang, M. Notcutt, T. Zanon-Willette, S. M. Foreman, M. M. Boyd, S. Blatt, and J. Ye, "Compact, thermal-noise-limited optical cavity for diode laser stabilization at 1×10^{-15}," *Opt. Lett.*, vol. 32, no. 6, pp. 641–643, 2007. [Online]. Available: http://ol.osa.org/abstract.cfm?URI=ol-32-6-641

[15] P. G. Westergaard, J. Lodewyck, L. Lorini, A. Lecallier, E. A. Burt, M. Zawada, J. Millo, and P. Lemonde, "Lattice-induced frequency shifts in Sr optical lattice clocks at the 10^{-17} level," *Phys. Rev. Lett.*, vol. 106, no. 21, art. no. 210801, May 2011.

[16] G. K. Campbell, A. D. Ludlow, S. Blatt, J. W. Thomsen, M. J. Martin, M. H. G. de Miranda, T. Zelevinsky, M. M. Boyd, J. Ye, S. A. Diddams, T. P. Heavner, T. E. Parker, and S. R. Jefferts, "The absolute frequency of the ^{87}Sr optical clock transition," *Metrologia*, vol. 45, no. 5, pp. 539–548, 2008.

[17] A. D. Ludlow, T. Zelevinsky, G. K. Campbell, S. Blatt, M. M. Boyd, M. H. G. de Miranda, M. J. Martin, J. W. Thomsen, S. M. Foreman, J. Ye, T. M. Fortier, J. E. Stalnaker, S. A. Diddams, Y. Le Coq, Z. W. Barber, N. Poli, N. D. Lemke, K. M. Beck, and C. W. Oates, "Sr lattice clock at 1×10^{-16} fractional uncertainty by remote optical evaluation with a Ca clock," *Science*, vol. 319, no. 5871, pp. 1805–1808, 2008. [Online]. Available: http://www.sciencemag.org/cgi/content/abstract/319/5871/1805

[18] A. V. Taichenachev, V. I. Yudin, V. D. Ovsiannikov, V. G. Pal'chikov, and C. W. Oates, "Frequency shifts in an optical lattice clock due to magnetic-dipole and electric-quadrupole transitions," *Phys. Rev. Lett.*, vol. 101, no. 19, art. no. 193601, Nov. 2008.

[19] S. Porsev, A. Ludlow, M. Boyd, and J. Ye, "Determination of Sr properties for a high-accuracy optical clock," *Phys. Rev. A*, vol. 78, no. 3, art. no. 032508, 2008.

[20] T. Middelmann, C. Lisdat, S. Falke, J. Winfred, F. Riehle, and U. Sterr, "Tackling the blackbody shift in a strontium optical lattice clock," *IEEE Trans. Instrum. Meas.*, vol. 60, no. 7, pp. 2550–2557, Jul. 2011.

[21] V. D. Ovsiannikov, A. Derevianko, and K. Gibble, "Rydberg spectroscopy in an optical lattice: Blackbody thermometry for atomic clocks," *Phys. Rev. Lett.*, vol. 107, art. no. 093003, Aug. 2011. [Online]. Available: http://link.aps.org/doi/10.1103/PhysRevLett.107.093003

[22] B. Young, F. Cruz, W. Itano, and J. Bergquist, "Visible lasers with subhertz linewidths," *Phys. Rev. Lett.*, vol. 82, no. 19, pp. 3799–3802, May 1999.

[23] Y. Y. Jiang, A. D. Ludlow, N. D. Lemke, R. W. Fox, J. A. Sherman, L. S. Ma, and C. W. Oates, "Making optical atomic clocks more stable with 10^{-16}-level laser stabilization," *Nat. Photonics*, vol. 5, no. 3, pp. 158–161, Jan. 2011.

[24] A. Quessada, R. Kovacich, I. Courtillot, A. Clairon, G. Santarelli, and P. Lemonde, "The Dick effect for an optical frequency standard," *J. Opt. B*, vol. 5, no. 2, pp. S150–S154, 2003.

[25] T. Legero, T. Kessler, and U. Sterr, "Tuning the thermal expansion properties of optical reference cavities with fused silica mirrors," *J. Opt. Soc. Am. B*, vol. 27, no. 5, pp. 914–919, 2010.

[26] K. Numata, A. Kemery, and J. Camp, "Thermal-noise limit in the frequency stabilization of lasers with rigid cavities," *Phys. Rev. Lett.*, vol. 93, no. 25, art. no. 250602, Dec. 2004.

[27] M. Notcutt, L.-S. Ma, A. D. Ludlow, S. M. Foreman, J. Ye, and J. L. Hall, "Contribution of thermal noise to frequency stability of rigid optical cavity via hertz-linewidth lasers," *Phys. Rev. A*, vol. 73, no. 3, art. no. 031804, 2006. [Online]. Available: http://link.aps.org/abstract/PRA/v73/e031804

[28] G. Harry, A. Gretarsson, P. Saulson, S. Kittelberger, S. Penn, W. Startin, S. Rowan, M. Fejer, D. Crooks, G. Cagnoli, J. Hough, and N. Nakagawa, "Thermal noise in interferometric gravitational wave detectors due to dielectric optical coatings," *Class. Quantum Gravity*, vol. 19, no. 5, pp. 897–917, 2002.

[29] V. Braginsky, "Thermodynamical fluctuations in optical mirror coatings," *Phys. Lett. A*, vol. 312, no. 3–4, pp. 244–255, May 2003.

[30] M. Cerdonio, L. Conti, A. Heidmann, and M. Pinard, "Thermoelastic effects at low temperatures and quantum limits in displacement measurements," *Phys. Rev. D*, vol. 63, no. 8, art. no. 082003, Mar. 2001.

[31] M. Evans, S. Ballmer, M. Fejer, P. Fritschel, G. Harry, and G. Ogin, "Thermo-optic noise in coated mirrors for high-precision optical measurements," *Phys. Rev. D*, vol. 78, no. 10, art. no. 102003, 2008.

[32] L. Chen, J. L. Hall, J. Ye, T. Yang, E. Zang, and T. Li, "Vibration-induced elastic deformation of Fabry-Perot cavities," *Phys. Rev. A*, vol. 74, no. 5, art. no. 053801, 2006. [Online]. Available: http://link.aps .org/abstract/PRA/v74/e053801

[33] J. Millo, D. Magalhães, C. Mandache, Y. Le Coq, E. English, P. Westergaard, J. Lodewyck, S. Bize, P. Lemonde, and G. Santarelli, "Ultrastable lasers based on vibration insensitive cavities," *Phys. Rev. A*, vol. 79, no. 5, art. no. 053829, May 2009.

[34] S. A. Webster, M. Oxborrow, and P. Gill, "Vibration insensitive optical cavity," *Phys. Rev. A*, vol. 75, no. 1, art. no. 011801, 2007.

[35] D. R. Leibrandt, M. J. Thorpe, M. Notcutt, R. E. Drullinger, T. Rosenband, and J. C. Bergquist, "Spherical reference cavities for frequency stabilization of lasers in non-laboratory environments," *Opt. Express*, vol. 19, no. 4, pp. 3471–3482, 2011.

[36] C. Lisdat, J. S. R. V. Winfred, T. Middelmann, F. Riehle, and U. Sterr, "Collisional losses, decoherence, and frequency shifts in opti-cal lattice clocks with bosons," *Phys. Rev. Lett.*, vol. 103, no. 9, art. no. 090801, Aug. 2009.

[37] S. Blatt, J. W. Thomsen, G. K. Campbell, A. D. Ludlow, M. D. Swallows, M. J. Martin, M. M. Boyd, and J. Ye, "Rabi spectroscopy and excitation inhomogeneity in a one-dimensional optical lattice clock," *Phys. Rev. A*, vol. 80, no. 5, art. no. 052703, Nov. 2009.

[38] K. Gibble, "Decoherence and collisional frequency shifts of trapped bosons and fermions," *Phys. Rev. Lett.*, vol. 103, no. 11, art. no. 113202, 2009. [Online]. Available: http://link.aps.org/abstract/PRL/v103/e113202

[39] A. M. Rey, A. V. Gorshkov, and C. Rubbo, "Many-body treatment of the collisional frequency shift in fermionic atoms," *Phys. Rev. Lett.*, vol. 103, no. 26, art. no. 260402, Dec. 2009.

[40] Z. Yu and C. J. Pethick, "Clock shifts of optical transitions in ultra-cold atomic gases," *Phys. Rev. Lett.*, vol. 104, no. 1, art. no. 010801, Jan. 2010.

[41] Y. B. Band and I. Osherov, "Collisionally induced atomic clock shifts and correlations," *Phys. Rev. A*, vol. 84, no. 1, art. no. 013822, Jul. 2011.

[42] D. J. Wineland and W. M. Itano, "Laser cooling of atoms," *Phys. Rev. A*, vol. 20, no. 4, pp. 1521–1540, Oct. 1979.

[43] M. Bishof, Y. Lin, M. D. Swallows, A. V. Gorshkov, J. Ye, and A. M. Rey, "Resolved atomic interaction sidebands in an optical clock transition," *Phys. Rev. Lett.*, vol. 106, no. 25, art. no. 250801, Jun. 2011.

[44] N. D. Lemke, J. von Stecher, J. A. Sherman, A. M. Rey, C. W. Oates, and A. D. Ludlow, "p-Wave cold collisions in an optical lattice clock," *Phys. Rev. Lett.*, vol. 107, art. no. 103902, 2011.

[45] J. Lodewyck, private communication, Sep. 2011.